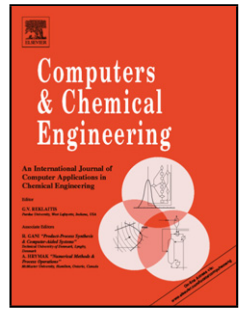

Title: Simulation of magnetic suspensions for HGMS using CFD, FEM and DEM modeling

Author: <ce:author id="aut0005"> Johannes Lindner<ce:author id="aut0010"> Katharina Menzel<ce:author id="aut0015"> Hermann Nirschl

PII:	S0098-1354(13)00077-X
DOI:	http://dx.doi.org/doi:10.1016/j.compchemeng.2013.03.012
Reference:	CACE 4669
To appear in:	*Computers and Chemical Engineering*
Received date:	21-9-2012
Revised date:	11-2-2013
Accepted date:	11-3-2013

Please cite this article as: Lindner, J., Menzel, K., & Nirschl, H., Simulation of magnetic suspensions for HGMS using CFD, FEM and DEM modeling, *Computers and Chemical Engineering* (2013), http://dx.doi.org/10.1016/j.compchemeng.2013.03.012

Simulation of magnetic suspensions for HGMS using CFD, FEM and DEM modeling

Johannes Lindner, Katharina Menzel, Hermann Nirschl

Institute of Mechanical Process Engineering and Mechanics, Karlsruhe Institute of Technology, Germany

Johannes.Lindner@kit.edu; Hermann.Nirschl@kit.edu

Phone: 0049/721/608-42427; Fax: 0049/721/608-42403

Abstract

Properties of magnetic suspensions depend on the fluid, the particles and the magnetic background field. The simulation is aimed at understanding the influence of magnetic properties in High Gradient Magnetic Separation processes. In HGMS magnetic particles are collected on magnetic wires for separation. External magnetic forces are calculated or simulated using the Finite Element Method and embedded first in a Computational Fluid Dynamics simulation. In the simulation, elliptic and rectangular wires aligned in field direction reach higher separation efficiencies than cylindrical wires. Magnetic forces from FEM with implemented dipole forces in a Discrete Element Method code show magnetically induced agglomeration and yield an acceptable agreement with experiments. Particle deposition on wires is investigated under the influence of different parameters. The porosity of the deposit is dependent on the magnetization of the wire and particles. A centrifugal force of 60 g has an important influence.

Highlights

- Finite Element Modeling simulation read in Computational Fluid Dynamics for magnetic particle tracks
- Discrete Element Modeling of magnetic particle chains

- Simulation of magnetic fluids

Keywords: CFD, DEM, FEM, HGMS, particle process

1. Introduction

The viscosity of magnetic suspensions is highly anisotropic and can be set externally by changing the magnetic field [1]. It is therefore interesting to simulate the behavior of magnetic suspensions for a better understanding of particle agglomerate porosity and shape, particle motion during separation, the possibility of particle displacement in the magnetic field under centrifugal force, and the separation of particles by magnetic forces to wires of rectangular shape. The separation efficiency of wires is necessary for an optimization of the specific High Gradient Magnetic Separation (HGMS) process.

HGMS has been used for many years to remove magnetic solids from fluid flow. It has become a standard method since its invention in 1937 by Frantz. Usually, the particles are separated by wires in the fluid, which are magnetized by an external magnetic field [2]. An application is the use of functionalized particles with a magnetic core in downstream processing of biotechnological processes. Eichholz et al. separated lysozyme from hen egg white by magnetic cake filtration [3]. HGMS is applied in wastewater treatment [2] or for the separation of ferrous contaminants from oil [4].

The aim is the simulation of the HGMS process. Using existing equations, it is possible to calculate the magnetic force acting on a particle and, hence, the particle flow in Computational Fluid Dynamics (CFD) [5]. Okada et al. used CFD simulation to determine the separation efficiency of different wire arrangements [6]. Hournkumnuard et al. used a Finite Difference Method to simulate concentration distributions [7]. Elliptic wire shapes were investigated by Li et al. [8].

Analytical approaches are limited to elliptical geometries. While round geometries are used in many applications, another shape of the separating device is chosen in some cases. Hayashi et al. [9] simulated the magnetic field and the fluid using Finite Element Modeling (FEM) and calculated the particle trajectory by solving the equation of motion for a rectangular wire shape. From this, they deduced the particle capture area in their specific experiment. An example of the use of different wire shapes is Magnetically Enhanced Centrifugation (MEC) [9]: the separating device is structured by laser cutting, resulting in a rectangular shape. The investigation of this shape and its influence on separation is in the focus of this article. The reason for creating structured wires lies in the process itself: in MEC the wire is cleaned by centrifugation during magnetic filtration. This allows in theory for a continuous process. The magnetic forces extend the time magnetic particles stay in the centrifuge by capturing them on a wire. Particles agglomerate on the wire and upper layers are removed by centrifugation. This requires star-shaped matrices which are produced most easily by laser cutting. CFD simulations of centrifuges have already been made, particle tracks in centrifuges have already been calculated [10, 11].

In this paper the magnetic field is modeled by FEM simulation. Fluid flow is simulated by CFD using a finite volume grid. The magnetic field is read into the CFD grid to determine the magnetic and fluid forces acting on a particle at each position. In comparison to the common analytical calculation, the advantage of this method lies in the fact that any geometry of a magnetic field can be calculated. In particular, it is possible to calculate magnetic wires of irregular shape as well as wires that are located too closely to each other for a simple addition of the magnetic forces.

Understanding of particle agglomerate building allows comprehension of different effects we face in the process such as strongly changing porosity under different conditions, notably different field strength or particle remanence. Another important effect is the particular deposit shape on magnetic wires. Satoh [12] studied ferromagnetic colloidal dispersions of clusters of ferromagnetic particles. The same formulae are now used in this paper to simulate interparticle forces. Fei Chen simulated magnetic deposit on wires using the Discrete Element Method (DEM) in a 2D approach [13]. DEM is used to simulate interparticle forces and agglomeration. A review on DEM is given in [14, 15]. Magnetic forces between particles are simulated analytically. Deposition of particles on a wire was simulated based on an analytical solution for the wire force acting on particles or a FEM vector field read into the DEM simulation. Numeric simulation is the only way to investigate the behavior of particles in an irregular magnetic field created at wire edges. The present paper focuses on the simulation of magnetic particles in general and in combination with centrifuges. An overview over simulation approaches and information flow is given in Figure 1.

Figure 1: Simulation methods and scale

2. Theory

We read magnetic fields simulated by FEM into a CFD simulation, and into a DEM simulation. For the latter several assumptions and simplifications were taken in our modeling approach of the Discrete Element Model:

1. Magnetic particles may be approached by a magnetic dipole despite not having an infinitesimal small core.
2. The approximation of the field around more than one dipole is not exact, as they interfere and soften or strengthen each other's magnetic field. We only took into account the direct neighboring particle in particle chains, which is physically not correct yet showed to be necessary to achieve a stable simulation.
3. Influence of hydrodynamic forces change kinetics but not final particle deposit shape and stability to centrifugal forces.
4. Surface forces including capillary forces may be neglected. This results for the investigated particle sizes of a force comparison.
5. Magnetic matter distorts the field. However to simplify the model, we assume magnetic particles to be aligned in direction of the external field.

It is obvious that the assumptions limit the universal validity of the model. The first and second assumption concern stability of the final model. Stability showed to be demanding, which is common in DEM. However an approximation of the physical behavior seems to be possible.

2.1 The Discrete Element Method

DEM consists in solving Newtonian equations for each single particle. In this case m_i is the mass of the particle, J_i the moment of inertia, r_i the position and ω_i the position angle. The second derivative is the translational or angular acceleration and $F_{i,k}$ and $T_{i,k}$ are forces and moments acting on the particle.

$$\sum_k F_{i,k} = m_{m,i} \frac{d^2 r_i}{dt^2} \quad (1)$$

$$\sum_k T_{i,k} = \overline{\overline{J_i}} \frac{d\omega_i}{dt} \quad (2)$$

A possible solution is discretization by a truncated Taylor series, for example in the velocity Verlet algorithm [16]:

$$r_i(t + \Delta t) = r_i(t) + \Delta t v_i(t) + \frac{\Delta t^2}{2m_{m,i}} \sum_k F_{i,k}(t) \quad (3)$$

$$v_i(t + \Delta t) = v_i(t) + \frac{\Delta t}{m_{m,i}} \sum_k F_{i,k}(t) \quad (4)$$

In a soft-sphere approach the overlap δ is determined from the particle diameters d_i and d_j, and the distance from the particle centre. A force of repulsion is implemented depending on the particle overlap. A soft sphere model allows equilibrating attracting and repelling forces over a time span. Use of a hard sphere model is in this case not possible because it does not allow rearranging of particles within the agglomerate. In the simulation contact of a virtual magnetic diameter for magnetic forces and contact of the physical spheres for mechanic forces is determined.

$$\delta = \begin{cases} \frac{d_i + d_j}{2} - r_{ij} & for\, r_{ij} < \frac{d_i + d_j}{2} \\ 0 & otherwise \end{cases} \quad (5)$$

2.1 Magnetic forces

Magnetic forces were implemented for the attraction of particles by a wire and for forces in between particles.

2.1.1 Introduction to magnetic forces

The magnetic flux density *B* is calculated from the magnetic field strength *H*:

$$\boldsymbol{B} = \mu_r \mu_0 \mathbf{H} = \mu_0 (\mathbf{H} + \mathbf{M}) \quad (6)$$

μ_0 is the permeability constant and μ_r the specific permeability of the material. Magnetization M is defined by the material susceptibility κ and the geometrical demagnetization factor D_m being 0.27 for a cylinder and 1/3 for a sphere [2]:

$$\boldsymbol{M} = \kappa \boldsymbol{H}_0 = \frac{\kappa_{im}}{1+D_m \kappa_{im}} \boldsymbol{H}_0 \xrightarrow{for\ \kappa_{im} \gg 1} \frac{\boldsymbol{H}_0}{D_m} \quad (7)$$

Separation of magnetic particles is described by identifying magnetic forces and fluid forces. The magnetic force F_m acting on a particle of the magnetic moment μ_P in the background field *H* is given by equation given by Rosensweig [17]:

$$\partial \boldsymbol{F}_m = \mu_0 (\mathbf{M_P} \cdot \nabla) \boldsymbol{H} \partial V_P \quad (8)$$

The torque is expressed as:

$$\partial \boldsymbol{T}_m = \mu_0 \mathbf{M_P} \times \boldsymbol{H} \partial V_P \quad (9)$$

For a field and a particle aligned in the same direction, the force F_m is written as a function of the magnetic field norm *H* [2]:

$$\boldsymbol{F}_m = \mu_0 V_P M_P \nabla H \quad (10)$$

The magnetic moment is the product of the particle volume V_P and the mean particle magnetization M_P.

2.1.2 External magnetic forces caused by cylindrical wires

By introducing the equation of the magnetic field around a cylinder published by Straton [18] and differentiating, the force of a magnetic cylinder on a magnetic particle is deduced in cylindrical coordinates *r* and θ [5]:

$$\boldsymbol{F}_m = \frac{1}{2}\mu_0 \Delta\kappa V_P \frac{\partial H^2}{\partial r} = -\mu_0 V_P M_P M_W \frac{a^2}{r^3}\begin{pmatrix} \frac{a^2}{r^2} + \cos(2\theta) \\ \sin(2\theta) \\ 0 \end{pmatrix}_{(r,\theta,z)} \qquad (11)$$

M_W is the magnetization of the wire and a the wire's diameter. $\kappa = M / (2H_0)$ is a material-dependent function calculated from the magnetization and the magnetic background field. This type of magnetic force is easy to program and sufficient for a first calculation of particles close to a single cylindrical wire.

The fluid drag force F_W on micron-sized particles ($Re<1$) is:

$$\boldsymbol{F}_W = -3\pi\eta d\boldsymbol{v} \qquad (12)$$

with the viscosity η, the particle diameter d and the relative velocity v between the particle and the fluid.

By balancing the magnetic force and the fluid resistance, the velocity of a particle is be calculated in cylindrical coordinates *r* and θ [5]:

$$\boldsymbol{v}_m = \frac{1}{18}\frac{d^2\mu_0 M_P M_D}{\eta}\frac{a^2}{r^3}\alpha\left[\frac{\left(\frac{a^2}{r^2}\alpha + \cos(2\theta)\right)\boldsymbol{e}_r - (\sin(2\theta))\boldsymbol{e}_\theta}{\sqrt{1 + \frac{a^4}{r^4}\alpha^2 + 2\frac{a^2}{r^2}\alpha\cos(2\theta)}}\right] \qquad (13)$$

with $\alpha = \frac{\mu_p - \mu_f}{\mu_p + \mu_f}$ (14)

In literature M_P is sometimes expressed as product of κ and H_0. This is true for paramagnetic material and for ferromagnetic materials at low field strengths. However in case of ferromagnetic materials at high magnetic field strengths and hence at saturation magnetization, a constant is replaced by two variables. Consequently, the more general magnetization M_P is preferred here. Watson [19] introduced this equation in a simplified form at the maximum radial velocity by setting the specific coordinates *r=a* and θ*=0*. For a fluid with low permittivity, α tends to one. An approximate analytical solution for the capturing radius was deduced by Gerber and Birss [5] for the longitudinal configuration based on the simplified equation of v_m:

$$\frac{R_c}{a} = \begin{Bmatrix} \frac{3}{4}\sqrt{3}\left|\frac{v_m}{v_0}\right|^{1/3}\left(1-\frac{2}{3}\left(\frac{v_m}{v_0}\right)^{-2/3}\right) & if\left(\frac{v_m}{v_0} > \sqrt{2}\right) \\ \frac{1}{2}\frac{v_m}{v_0}\left(\sqrt{1-K^2}+K(\pi-\arccos(K)\right) & if\left(\frac{v_m}{v_0} < \sqrt{2}\right) \end{Bmatrix} \quad (15)$$

Similar models were developed and provide similar results [20, 21]. Hence in our approach, the flow of a particle in the surroundings of a single cylindrical wire was calculated analytically as well as by implementing magnetic forces in CFD simulation. Determination of the particle tracks around non-elliptic wires, by contrast, cannot be done analytically. Rectangular shapes are simulated by FEM. Furthermore, multiple wires at low distance cannot be calculated by summing up the forces because of the non-linearity of the magnetic field. This aggravates analytical solution.

2.1.3 Interparticle magnetic forces

Interparticle forces are active over a limited radius around the particle for reduction to fourth power. Here, calculation of magnetic forces is limited to a specific distance around the particle to save calculation time. In the simulation of Figure 7 and Figure 8 the radius is four times the physical particle radius, but reduced to a very narrow region of 1.5 times the particle radius in the simulation of particle deposition. This saves computational power and allows for the simulation of a larger particle number. The magnetic forces acting between two dipoles of the moments m_{Pi} and m_{Pj} and the distance *r* are used for the approximation of the magnetic forces of two magnetic spheres. Rosensweig gives the formula for the potential *E* between particles *i* and *j*:

$$E = \frac{\mu_0 m_{Pi} m_{Pj}}{4\pi r^3}\left(\boldsymbol{n}_i \cdot \boldsymbol{n}_j - 3(\boldsymbol{n}_i \cdot \boldsymbol{t}_{ij})(\boldsymbol{n}_j \cdot \boldsymbol{t}_{ij})\right) \quad (16)$$

The potential depends on the orientation of the magnetic particle moments n_i and n_j relative to each other and to the vector from particle *i* to *j* t_{ij}. The formula was evaluated by Satoh [12] for the force $F_{m,ij}$:

$$\boldsymbol{F}_{m,ij} = -\frac{3\mu_0 m_{Pi} m_{Pj}}{4\pi d^4} * \frac{1}{\left(r_{ij}/d\right)^4}\left[-\left(\boldsymbol{n}_i * \boldsymbol{n}_j\right) + 5\left(\boldsymbol{n}_i * \boldsymbol{t}_{ij}\right)\left(\boldsymbol{n}_j * \boldsymbol{t}_{ij}\right)\boldsymbol{t}_{ij} - \left\{\left(\boldsymbol{n}_j * \boldsymbol{t}_{ij}\right)\boldsymbol{n}_i + \left(\boldsymbol{n}_i * \boldsymbol{t}_{ij}\right)\boldsymbol{n}_j\right\}\right] \tag{17}$$

The moment $T_{m,ij}$ on a magnetic particle is:

$$\boldsymbol{T}_{m,ij} = -\frac{\mu_0 m_{Pi} m_{Pj}}{4\pi d^4} * \frac{1}{\left(r_{ij}/d\right)^3}\left\{\boldsymbol{n}_i \times \boldsymbol{n}_j - 3\left(\boldsymbol{n}_j * \boldsymbol{t}_{ij}\right)\boldsymbol{n}_i \times \boldsymbol{t}_{ij}\right\} \tag{18}$$

Now, the magnetic particles are assumed to be directed in field direction. The Cartesian product in the same direction is zero. Hence, the moments resulting from both different particles and the magnetic field are neglected. The force was simplified under the assumption of the particles being aligned in x-direction of a constant magnetic field with the components of the direction vector t_x, t_y and t_z:

$$\boldsymbol{F}_{m,ij} = -\frac{3\mu_0 m_{Pi} m_{Pj}}{4\pi}\frac{1}{r_{ij}^4}\begin{pmatrix}(5 * t_X{}^2 - 3)t_X \\ (5 * t_X{}^2 - 1)t_Y \\ (5 * t_X{}^2 - 1)t_Z\end{pmatrix} \tag{19}$$

Under the same assumption of aligned particles, torsion is neglected in this simulation.

2.2 Non-magnetic forces

2.2.1 Mechanic forces

The mechanic interparticle forces were introduced by Mindlin. In our case, the mechanical forces counteract attracting magnetic forces and allow for a stable equilibrium to simulate magnetically induced agglomeration. Mechanical forces are divided into spring and damper forces. The spring force and damper force in normal direction $F_{n,ij}$ are as follows [22-24]:

$$\boldsymbol{F}_{n,ij} = k_n \delta^{3/2}\boldsymbol{n}_{ij} - \eta_{n,ij} * \boldsymbol{v}_{rel,n,ij} \tag{20}$$

with $k_n = \frac{E^* \sqrt{R^*}}{3(1-\nu^2)}$ (21)

and $\eta_{ij} = -c_n \sqrt{\frac{9}{2}\left(\frac{m_{m,i} m_{m,j}}{m_{m,i}+m_{m,j}}\right)\sqrt{\delta} k_n}$ (22)

The material parameters, spring constant k_n and the damper constant $\eta_{n,ij}$, are difficult to determine in the case of µm-sized particles. Hence, they are calculated from material properties. However, the overlap δ adapts to achieve equilibrium, which results in magnetic agglomeration independently of particle stiffness. The tangential damper force is:

$\boldsymbol{F}_{t,ij} = -\eta_{t,ij} * \boldsymbol{v}_{relt,ij}$ (23)

with $\eta_{t,ij} = c_n \sqrt{\frac{9}{2} \frac{m_{m,i} * m_{m,j}}{m_{m,i}+m_{m,j}} \sqrt{\delta} k_n}$ (24)

with c_n=0.3 [25]. This force is necessary to prevent oscillation of one particle around the region of highest magnetic field of another particle. The coefficients have been chosen according to [26]. Flow resistance of a single particle in a laminar regime according to Stokes is given in (6). A summary of DLVO forces introduced in [27] did not show significant differences in the simulation.

2.2.2 The centrifugal force

Magnetically enhanced centrifugation is an important use of the simulation. The influence of the wire force is simulated to identify possibilities to clean the wire. The centrifugal force F_Z is implemented as constant acceleration in wire direction. The centrifugal force at the wire end is implemented for the whole simulation area as constant r for simplicity. It is calculated from centrifugal velocity ω.

$\boldsymbol{F}_Z = m_m * \omega^2 * \boldsymbol{r}$ (25)

Centrifugal force is normalized to the gravitational force to eliminate units:

$C = \frac{\omega^2 * r}{g}$ (26)

3. Simulation methods

3.1 Methods to simulate magnetic wire forces

Simulation of the magnetic field by FEM

Particle separation was simulated from wires of elliptic and rectangular shape of the same cross section area but different semi-axis. For this purpose the magnetic field was determined by FEM (Comsol Version 3.4) and read into a CFD code to calculate forces on particles. The permeability was set to 1 for the fluid and 5 for the wire at the background field of 400 kA/m corresponding 0.5 T. Figure 2 (a) shows the FEM grid and the magnetic field around a rectangular wire. The corners of the rectangle are prone to numerical errors, which is limited to a very small area by a fine grid.

Figure 2: The FEM grid around a rectangular wire (a); the field and field gradient around a cylindrical wire (b)

Figure 2 (b) shows the field around a cylindrical wire. The colors indicate the field strength; there is a maximum in the horizontal field direction and a minimum perpendicular to the field direction. The resulting gradient is shown by the arrows. The field is attractive in background field direction left and right and repulsing perpendicular to the field. The gradient was calculated and then exported with the coordinates of each node.

Implementation of the magnetic forces in CFD

Ansys Fluent Version 12 was used to simulate the fluid flow around wires of different shape. The field gradient was read into Fluent. The node value of the magnetic field gradient in x and y direction was read into a CFD code and stored in the memory of the finite volume cells by assigning the closest value. An interpolation seemed not to be necessary by having sufficiently fine grids. The particle tracks of different wires were simulated using this approach. As discretization causes inaccuracies, the finite volume grid has to be fine near the wire similarly to the finite element grid. After simulation of the fluid flow the force on the particles was calculated from eq. (10) at discrete time steps. Fluid velocity is

1 mm/s, which is the same scale as in our HGMS experiments. Particle magnetization in this case is 1.26e6 A/m. This led to particle tracks around wires, which reflected the separation of particles.

3.2 Methods to simulate interparticle forces by DEM

The computer system used was Windows XP SP2. The computer was a quad core with 3.14 GHz, 64 bit and 8 GB Ram. As function implementation did not allow parallel simulation, simulations were performed on a single core. The software EDEM Version 2.3.1 of DEM Solutions was used as framework and for graphical view. The magnetic forces as well as the mechanic contact model were programmed in C and implemented in the simulation as user-defined library (UDL). Windows SDK 7.1 was used to compile the source code. Eq. (11) was implemented to simulate the force of the magnetic wire on the particles, except for simulations implementing the centrifugal force. To simulate the field on the wire end on centrifugal force influence, the magnetic field was read and implemented using eq (10). In the contact model, eq. (19) was implemented as the magnetic model. The mechanic model consisted of eqs. (20) and (23) with the parameters of eqs. (21), (22) and (24). As mentioned in the second assumption, magnetic forces were suppressed for distant particles in the same agglomerate. This eliminated instabilities, specifically particles in the middle of the wire being pushed out by neighboring particles. We suppose this instability to be consequence of the approximation of the magnetic particle core with a dipole equation (17) and the superposition of magnetic forces. Important values in the DEM simulation are given in Table 1.

Table 1: Values used in the DEM Simulation

Interparticle forces summarized in the DLVO theory usually are only important for particle sizes below µm-scale. According to [27] magnetic forces predominate over surface forces for the particle sizes simulated. A simulation, including the DLVO theory and fluid flow summarized in [27], was performed for particles of 1 µm in size, yet did not change the final shape of the deposit, hence DVLO and CFD forces were neglected in further simulations.

<u>Experimental Validation</u>

Validation is necessary to reveal shortcomings which are inevitable in every model or simulation. We decided to compare the deposit of magnetite particles on a ferrous wire in a magnetic field in air by pouring a small amount of particles over a wire in a magnetic field (see 4.2.1 Validation). The process of deposition could not be visualized in an experiment due to the low medium particle size of 2 µm and the high velocities during deposition in the range of several m/s. In comparison the time scale of the simulation was 50 ms. Simulation time itself was about 10 h. For particle deposition, a wire of 1 mm in diameter and 25 mm in length was used. The wire material was a ferromagnetic steel with the material number 1.4016 with a saturation magnetization of 1.3 * 10^6 A/m. The particles were iron oxide particles, named Bayoxid 8706, with a saturation magnetization of about 400 000 A/m.

4. Results and discussion

4.1 Results and discussion of FEM and CFD coupling

Birss et al. [28] give a formula for the attractive angle θ_c for cylindrical geometry. The angle specifies the limit between the attractive and the repelling zone on the wire surface:

$$\theta_c = arctan\left(\frac{1+K\frac{a^2}{r^2}}{1-K\frac{a^2}{r^2}}\right) \qquad (27)$$

For an elliptic geometry, θ_c decreases from 90° to 45° with rising r, the value of the force being very low at high distance. In a rectangular geometry, the angle determined in the simulation is 0° close to the wire and approaches 45° at high distance.

Figure 3: The radial field component versus the normalized field force $F_r/|F|$ for a cylindrical (a) and rectangular (b) wire shape

As seen in Figure 4, the capturing radius was normalized to the radius of a cylindrical wire for different ratios of height *h* to width *i*. The capturing radius may be approximated by a simple power function. The form of the function is:

$$\frac{R_C}{R_{C,cylinder}} = f * \left(\frac{h}{i}\right)^g \quad (28)$$

R_c is the capturing radius of the wire to be calculated and $R_{c,cylinder}$ the capturing radius of a wire of the same area, which was calculated by the formulae of Gerber/Birrs [5], Uchiyama/Hayashi [21] or Cowen [20]. The simulation suggests the following parameters for rectangular and elliptic geometries to approximate rectangular and elliptic shaped wires shown in Table 2.

Table 2: Empiric factors for irregular shapes determined by simulation

Figure 4: Capture radius of different wire shapes normalized to the cylindrical wire's capture radius plotted versus the relation length/width

As evident from Figure 4, the power function is an approximation. The lower capturing radius for a quadratic wire shape might be due to smaller gradients for a slightly unfavorable geometry as well as to a disadvantageous fluid flow around the wire compared to the more elongated geometries in fluid direction. Nevertheless, the formula represents an acceptable approximation for calculation purposes. The result is in line with experiments, showing that wire shapes arranged parallel to the field direction enhance separation slightly [29].

A wire of quadratic shape of specific edge length seemed to have a higher capturing radius than a cylindrical wire having a diameter corresponding to the edge length. Compared to the simulation, this seems to be primarily due to the fact that the quadratic wire has a larger cross-sectional area and, hence, higher mass rather than an effectively better geometry. In the simulation the advantage of the field gradient seems to be compensated by disadvantages in the flow.

As an outlook, the simulation size is limited by the assignment of FEM node values to VFM cell values. The number of operations is the product of the numbers of FEM nodes and FVM cells. Hence, for very large grids, the reading procedure is extended dramatically, complicating 3-dimensional simulation. To improve the simulation, an approach performing both simulations on a single grid seems to be the best way to handle 3-dimensional geometries.

4.2 Results and discussion of the DEM model

Simulation of particle trajectories is not sufficient to describe the behavior of magnetic suspensions due to the influence of particles on each other. Experiments show needle-shaped magnetically induced agglomeration of particles. Velocities of particles in the vacuum are high and strongly reduced when the drag model is implemented. The same behavior appears in the simulation. The attraction zones simulated in the FEM model allow for particle agglomeration only on the two sides of a particle aligned in field direction (see Figure 2).

4.2.1 Validation

For experimental validation, a small amount of particles was poured over the wire, resulting in the deposit shown in Figure 5 (a). The medium particle diameter was 2 µm, as was measured by laser diffraction. Figure 5 (b) shows a simulation based on 100 µm particles. The final image looks similar, despite the different particle size. A simulation close to the real particle size was not possible due to the huge particle amount necessary. In the simulation 500 particles were simulated.

The most obvious difference is the circular deposit in the experiment compared to the simulation. The reason is the change of the field direction of the wire which we neglected due to assumption 5. This was necessary so the model could be simplified in eq. (19). To avoid this inaccuracy in a future simulation, particle rotation has to be permitted and the field direction change of wire and surrounding particles has to be implemented based on equations (17) and (18). This results in a more sophisticated and computationally expensive model. The shape of the deposit, densely packed close to the wire and porous in upper layers, is in the simulation in good agreement with the experiment.

Figure 5: Agglomeration of Bayoxid particles on a wire (a) and simulation of 100 µm particles on a 1 mm wire (b)

<u>Comparison with other simulations</u>

Our simulation shall now be compared with a simulation of other researchers. For comparison, we plotted an image published by Fei Chen [13]. He simulated the influence of centrifugal force on particle deposition. A similar simulation is explained in detail and compared with the simulation in Figure 10. Acceleration was calculated from the rotational velocity of 1500 rpm as 60 g. The simulation was done in 2D contrary to our simulation in Figure 10. Agreement of Figure 6 (a) and Figure 6 (b) was not ideal at the end of the wire. In our simulation, there are no particles beyond the end of the wire. This difference may be caused by a difference in the simulation of the magnetic field by FEM. The magnetic field resulting from our simulation had a steep decline at the end, resulting in huge repelling forces from this zone towards the wire on the left as well as towards the right at the right end of the zone. The steep end of the deposit at the wire end of Figure 6 (b) was due to the repelling forces of magnetic particles on each other perpendicular to the magnetic field, see Figure 3 (a). However, this was the only major difference to the Figure 6 (a).

Figure 6: 2D simulation of Fei Chen [13] (a); image of a simulation at 60 g for comparison (b)

4.2.2 Simulation results

Agglomeration

Interparticle agglomeration is an important aspect in the simulation of magnetic suspensions. The rheological behavior of particles as well as their settling velocity on a magnet depend to our knowledge on agglomeration. Hence, this element is important for the understanding of particle separation and its simulation is necessary for an accurate representation. Needle-shaped agglomeration is documented in literature [30]. A simulation implementing one large particle showed agglomeration of 100 µm particles on the surface of a significantly larger 1 mm particle (Figure 7). The characteristic needle-shaped deposit was visible in this simulation. Particles agglomerated in particular at one end of the large particle and formed needles. More important than the agglomeration on the large particle is the agglomeration of monodisperse particles.

Figure 7: Particle agglomeration of 100 µm particles near one 1 mm particle

Wire deposit

Usually, magnetic wires are made of ferromagnetic steel, while the particles have a magnetite core. The magnetization of the wire is far higher than the magnetization of the particles. However, in case of larger particle magnetization or at a large distance from the wire, the shape and porosity of the agglomerate changed significantly in our simulation. For comparison, we simulated different magnetizations to show the influence on the cake structure.

The magnetic force of a wire was implemented in this simulation. In combination with the interparticle forces, the particle deposit on a wire was simulated. The simulation showed a needle-shaped or a dense particle cake, depending on the magnetization of the wire to that of the particle. In Figure 8 (a), a dense particle deposit is shown. In Figure 8 (b) and (c), the magnetization of the wire was reduced by a factor 70 from the value determined for the wire material. The shape of the deposit was different, showing a highly porous needle-shaped structure. It seems logical that the deposit depends on the ratio of the magnetic wire force and the interparticle force.

Figure 8: Agglomerates of 1 µm particles on an iron wire (a) and on a weakly magnetic wire (b), (c)

Size comparison of particles on a wire

A simulation on different particle sizes was performed (Figure 9). The deposit of 10 µm particles (a) and 20 µm particles (b) is virtually identical. For 100 µm particles (c), the deposit was similar. We expected this result out of the implemented equations. Due to these similarities, the size difference is not expected to be important in the validation. The final shape seems to be more dependent on different parameters like particle magnetization than on the particle size.

Figure 9: Comparison of particles of different sizes: 10 µm (a); 20 µm (b); 100 µm (c)

Influence of centrifugal force on wire deposit

The simulation of the magnetic field at the wire end by FEM allows calculating the sliding of particles under a gravitational or centrifugal field. This is important to simulate the behavior of particles in superposed centrifugation and magnetic separation. Magnetically enhanced centrifugation, which is one of our research areas, is used for the simultaneous separation and cleaning of a magnetic wire filter. In the centrifuge the height of the deposit depends on the centrifugal force. Centrifugal force is used to structure the deposit. The amount of particles caught on the wire depends as well on the centrifugal force. In the experiment the shape of the cake on the wire was uniform in the direction of the wire axis.

For this geometry, large gradients created high forces at the end, which retained the particles. In Figure 10 the wire simulation is shown for a field in vertical direction. The particle needles were aligned in field direction. A centrifugal force of 0, 10, 60 and 240 g, respectively, was applied. In this case, magnetic forces and friction counteracted centrifugal forces. The deposit slid to the outside in comparison with a uniform distribution without centrifugal force. Accuracy might be limited by the way forces are calculated (see assumption 2).

Figure 10: Magnetic field at the end of a wire simulated in FEM. Comparison of a wire end at 0 g (a), 10 g (b), 60 g (c) and 240 g (d).

The centre of gravity of the particle deposit in the simulation moved to the outside, which is shown in Figure 11. At 240 g, particles were mainly retained on the wire by the large gradients at the wire end. Hence, the particle centre of gravity was very close to the end. The large gradient at the wire end was the reason for the large displacement of the centre of gravity.

Figure 11: Diagram of the movement of the centre of gravity

Wire shape

Rectangular wires behaved similar to cylindrical wires in both experiment and simulation regarding the structure of the particle deposit, as well under centrifugal forces. However simulation of a wire of quadratic shape under centrifugal force was not as stable as the simulation of cylindrical wires, which might be a consequence of singular points on the edges in the vector field read from the FEM simulation. The amount of particles collected on the wire did not change significantly. The change in the capturing radius explained above is hence the main influence of changed shape.

5. Conclusion

Calculation of particle tracks around wires of different shapes is important to understand and optimize HGMS devices. Simulation was possible by combining numerical simulations of the magnetic field and fluid flow. The particle trajectories were calculated analytically. Elliptic and rectangular wires showed to be most efficient when aligned in field and flow direction, behaving slightly different to each other. The separation of these shapes could be approximated by a power function based on the equations for cylindrical wires.

The DEM simulation was a first approach to the direct modeling of magnetically induced agglomeration. Simulation showed the general behavior of magnetic particles. Specifically the needle-shape reported by different researchers could be reproduced in the simulation. Comparison of the experimental particle cake on a wire and the simulation revealed a satisfactory agreement. The simulation showed the specific behavior of particles, such as their rearrangement on the wire over time.

According to the simulation, the porosity and the cake structure of particles were completely different depending on the magnetization of particles and wire. In the case of wires in a centrifugal field, the height of the particle deposit on the wire depended on the centrifugal force. Simulation showed the highest deposit at the end of the wire. At 60 g, the height of deposit in the middle of the wire was limited. At 240 g, particles were only retained at the end of the wire.

Acknowledgements

We acknowledge funding of our work under the project MagPro2LIFE by the EU in the 7th Framework Program. The authors owe special thanks to the MagPro2LIFE consortium. Thanks to Ansys, Comsol and EDEM for support.

Symbols

Table 3: Symbols

List of abbreviations

MEC Magnetically Enhanced Centrifugation

HGMS High Gradient Magnetic Separation

DEM Discrete Element Method

FEM Finite Element Method

CFD Computational Fluid Dynamics

References

1. Zipser, L., L. Richter, and U. Lange, *Magnetorheologic fluids for actuators.* Sensors and Actuators A: Physical, 2001. 92(1-3): p. 318-325.
2. Svoboda, J., *Magnetic Techniques for the Treatment of Materials.* Kluwer Academic Publishers, 2004.
3. Eichholz, C., et al., *Recovery of lysozyme from hen egg white by selective magnetic cake filtration.* Engineering in Life Sciences, 2011. 11(1): p. 75-83.
4. Menzel, K., J. Lindner, and H. Nirschl, *Removal of magnetite particles and lubricant contamination from viscous oil by High-Gradient Magnetic Separation technique.* Separation and Purification Technology, 2011.
5. Gerber R., B.R.R., *High Gradient Magnetic Separation.* Research Studies Press, 1983.
6. Okada, H., et al., *Computational Fluid Dynamics Simulation of High Gradient Magnetic Separation.* Separation Science and Technology, 2005. 40(7): p. 1567-1584.
7. Hournkumnuard, K. and C. Chantrapornchai, *Parallel simulation of concentration dynamics of nano-particles in High Gradient Magnetic Separation.* Simulation Modelling Practice and Theory, 2011. 19(2): p. 847-871.
8. Li, X.L., et al., *The investigation of capture behaviors of different shape magnetic sources in the high-gradient magnetic field.* Journal of Magnetism and Magnetic Materials, 2007. 311(2): p. 481-488.
9. Hayashi, S., et al., *Development of High Gradient Magnetic Separation System for a Highly Viscous Fluid.* IEEE Transactions on Applied Superconductivity, 2010. 20(3): p. 945-948.
10. Spelter, L.E., J. Schirner, and H. Nirschl, *A novel approach for determining the flow patterns in centrifuges by means of Laser-Doppler-Anemometry.* Chemical Engineering Science, 2011. 66(18): p. 4020-4028.
11. Romaní Fernández, X. and H. Nirschl, *Multiphase CFD Simulation of a Solid Bowl Centrifuge.* Chemical Engineering & Technology, 2009. 32(5): p. 719-725.
12. Satoh, A., et al., *Stokesian Dynamics Simulations of Ferromagnetic Colloidal Dispersions in a Simple Shear Flow.* J Colloid Interface Sci, 1998. 203(2): p. 233-48.
13. Chen, F., *Magnetically Enhanced Centrifugation for Continuous Biopharmaceutical Processing.* Massachusetts Institute of Technology, 2009.

14. Zhu, H.P., et al., *Discrete particle simulation of particulate systems: Theoretical developments.* Chemical Engineering Science, 2007. 62(13): p. 3378-3396.
15. Zhu, H.P., et al., *Discrete particle simulation of particulate systems: A review of major applications and findings.* Chemical Engineering Science, 2008. 63(23): p. 5728-5770.
16. M.P., A., *Computer Simulation of Liquids.* Clarendon Press, Oxford, 1987.
17. Rosensweig, R.E., *Ferrohydrodynamics.* Courier Dover Publications, 1997.
18. Straton, J.A., *Electromagnetic Theory.* McGraw-Hill, New York, 1941.
19. Watson, J.H.P., *Magnetic filtration.* Journal of Applied Physics, 1973. 44(9): p. 4209.
20. Cowen, C., F. Friedlaender, and R. Jaluria, *Single wire model of high gradient magnetic separation processes I.* IEEE Transactions on Magnetics, 1976. 12(5): p. 466-470.
21. Uchiyama, S., Hayashi, K., *Analytical theory of magnetic particle capture process and capture radius in high gradient magnetic separation.* Industrial applications of magnetic separation: Proceedings of an International Conference, Rindge, 1978(IEEE: 78CH1447-2).
22. Deen, N.G., et al., *Review of discrete particle modeling of fluidized beds.* Chemical Engineering Science, 2007. 62(1-2): p. 28-44.
23. Langston, P.A., U. Tüzün, and D.M. Heyes, *Discrete element simulation of granular flow in 2D and 3D hoppers: Dependence of discharge rate and wall stress on particle interactions.* Chemical Engineering Science, 1995. 50(6): p. 967-987.
24. Simsek, E., et al., *An Experimental and Numerical Study of Transversal Dispersion of Granular Material on a Vibrating Conveyor.* Particulate Science and Technology, 2008. 26(2): p. 177-196.
25. Chu, K.W. and A.B. Yu, *Numerical simulation of complex particle–fluid flows.* Powder Technology, 2008. 179(3): p. 104-114.
26. Tsuji, Y., T. Tanaka, and T. Ishida, *Lagrangian numerical simulation of plug flow of cohesionless particles in a horizontal pipe.* Powder Technology, 1992. 71(3): p. 239-250.
27. Stolarski, M., et al., *Sedimentation acceleration of remanent iron oxide by magnetic flocculation.* China Particuology, 2007. 5(1-2): p. 145-150.
28. Birss, R., R. Gerber, and M. Parker, *Theory and design of axially ordered filters for high intensity magnetic separation.* IEEE Transactions on Magnetics, 1976. 12(6): p. 892-894.
29. Lindner, J., et al., *Efficiency Optimization and Prediction in High-Gradient Magnetic Centrifugation.* Chemical Engineering & Technology, 2010. 33(8): p. 1315-1320.
30. Vuppu, A.K., A.A. Garcia, and M.A. Hayes, *Video Microscopy of Dynamically Aggregated Paramagnetic Particle Chains in an Applied Rotating Magnetic Field.* Langmuir, 2003. 19(21): p. 8646-8653.

Table 4: Values used in the DEM Simulation

Denotation		Value (unless noted differently)	Unit
wire radius	a	0.5 e-3	[m]
Hamaker constant	A_H	6.5 e-20	[J]
particle radius	b	0.5e-6	[m]
particle diameter	d	5e-5	[m]
geometry constant	D_m	0.27(cylinder); 0.33 (sphere)	[-]
electron charge	e	1.602176487 e-19 C	[C=As]
Initial particle velocity	v	0.001	m/s
magnetic background field	H_0	4e5	[A/m]
magnetization particle	M_P	4.8e5 (susceptibility of magnetite)	[A/m]
saturation magnetization wire	M_W	1.7e6(susceptibility of iron)	[A/m]
dynamic viscosity	η	1000	[kg/m s]
inverse Debye length	κ_d	2e8	[1/m]

specific permeability	μ_r	1 (vacuum)	[-]
density particle	ρ_P	2000	[kg/m³]
kinematic viscosity	ν	1e-6 (water)	[m²/s]

Table 5: Empiric factors for irregular shapes determined by simulation

	Factor f	Exponent g
Elliptic geometry	0.9742	0.1828
Rectangular geometry	0.9802	0.1229

512 Table 6: Symbols

	Unit	Typical value	Denotation
a	[m]	0.5 e-3	wire radius
A_H	[J]	6.5 e-20	Hamaker constant
B	[T]		magnetic flux density
b	[m]	0.5e-6	particle radius
d	[m]	5e-5	particle diameter
D_m	[-]	0.27(cylinder); 0.33 (sphere)	geometry constant
e	[C = As]	1.602176487 e-19 C	electron charge
e_r, e_θ	[-]	1	unity vectors in cylindrical coordinates
F_m	[N]		magnetic force
H	[A/m]		Norm of the magnetic field
H_0	[A/m]	4e5	magnetic background field
J_i	[kg m²]		inertia tensor
K	[–]		auxiliary quantity
L	[m]		needle length
M	[A/m]		magnetization

M_P	[A/m]	4.8e5 (susceptibility of magnetite)	magnetization particle
M_W	[A/m]	1.7e6(susceptibility of iron)	saturation magnetization wire
$\boldsymbol{m_p}$	[A m²]	$=V_P*M_P$	magnetic moment
m_P	[A m²]	$=V_P*M_P$	normalized magnetic moment
m_m	[kg]		mass of particle
Rc	[m]		capturing radius
$\vec{r}$	[m]		distance vector
r	[m]		normalized distance vector, cylindrical coordinate
r_X, r_Y, r_Z,	[-]		components of $\vec{r}$
v	[m]		velocity relative to the fluid
v_0	[m/s]		fluid velocity
v_m	[m/s]		velocity of magnetic particle next to the wire
V_P	[m³]		volume particle
η	[kg/m s]	1000	dynamic viscosity
κ	[–]		volume susceptibility
κ_d	[1/m]	2e8	inverse Debye length

μ_r	[-]	1 (vacuum)	specific permeability
μ_0	[V s/A m]	4π e-7	permeability constant
μ_P	[A m²]		magnetic moment
ρ_P	[kg/m³]	2000	density particle
θ	[-]		angle, cylindrical coordinate
θ_c	[-]		Attractive angle
ε_0	[As/Vm]	$1/\mu_0 c_0^2$=8.85418781762e-12	permittivity
ε_r	[-]	1	specific permittivity
ν	[m²/s]	1e-6 (water)	kinematic viscosity

Figure 1

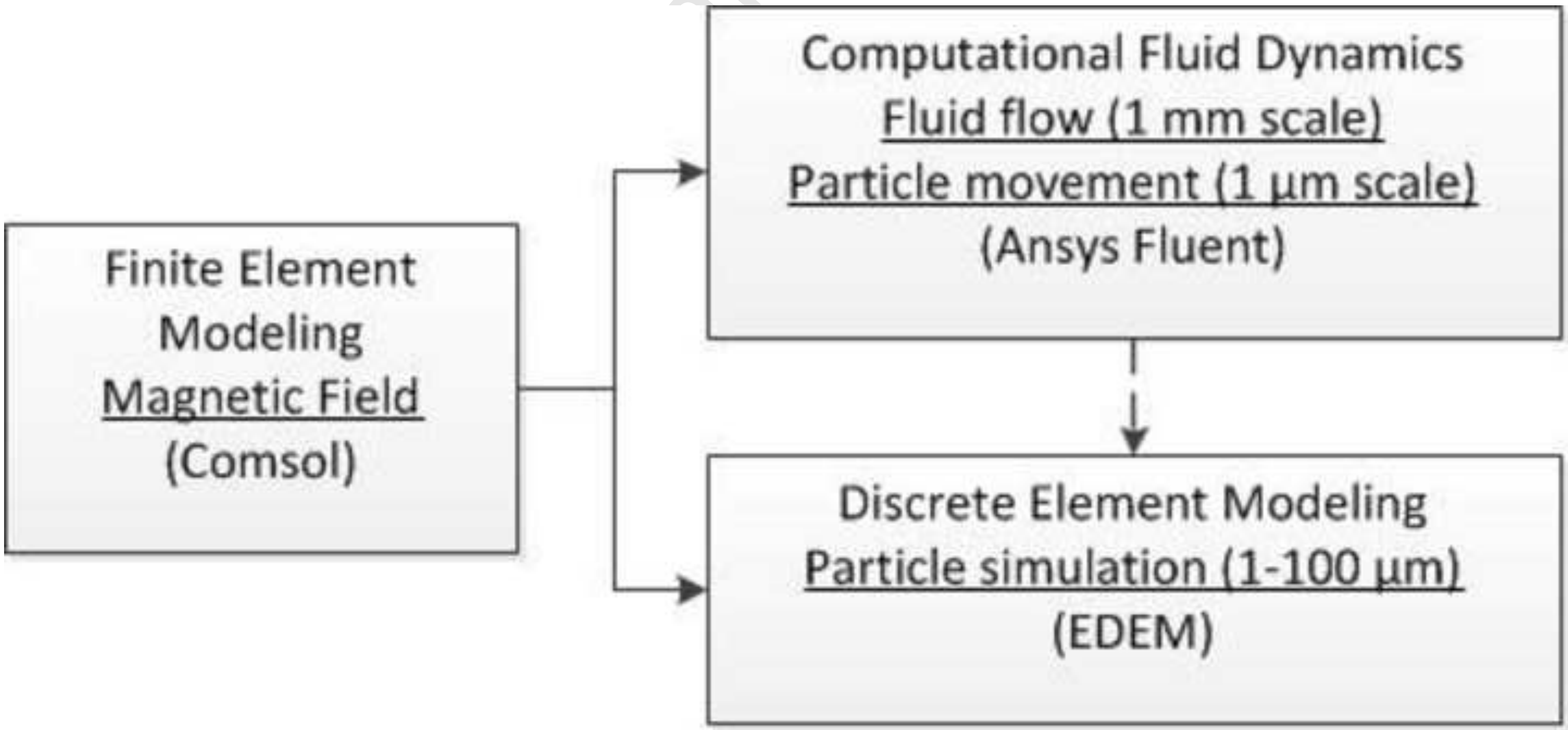

Computational Fluid Dynamics
Fluid flow (1 mm scale)
Particle movement (1 μm scale)
(Ansys Fluent)
Finite Element
Modeling
Magnetic Field
(Comsol)
Discrete Element Modeling
Particle simulation (1-100 μm)
(EDEM)

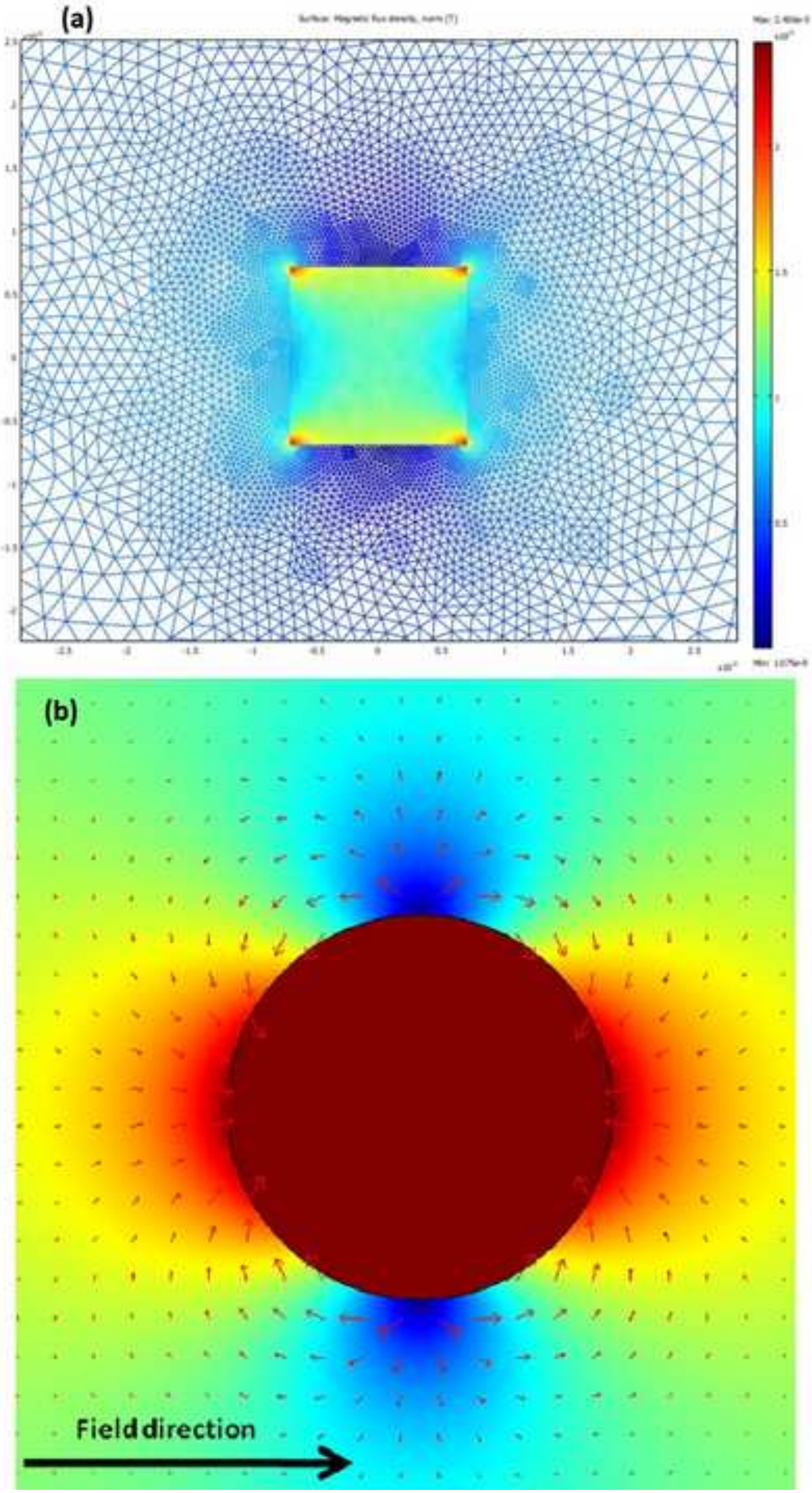
(a)
(b)
Field direction

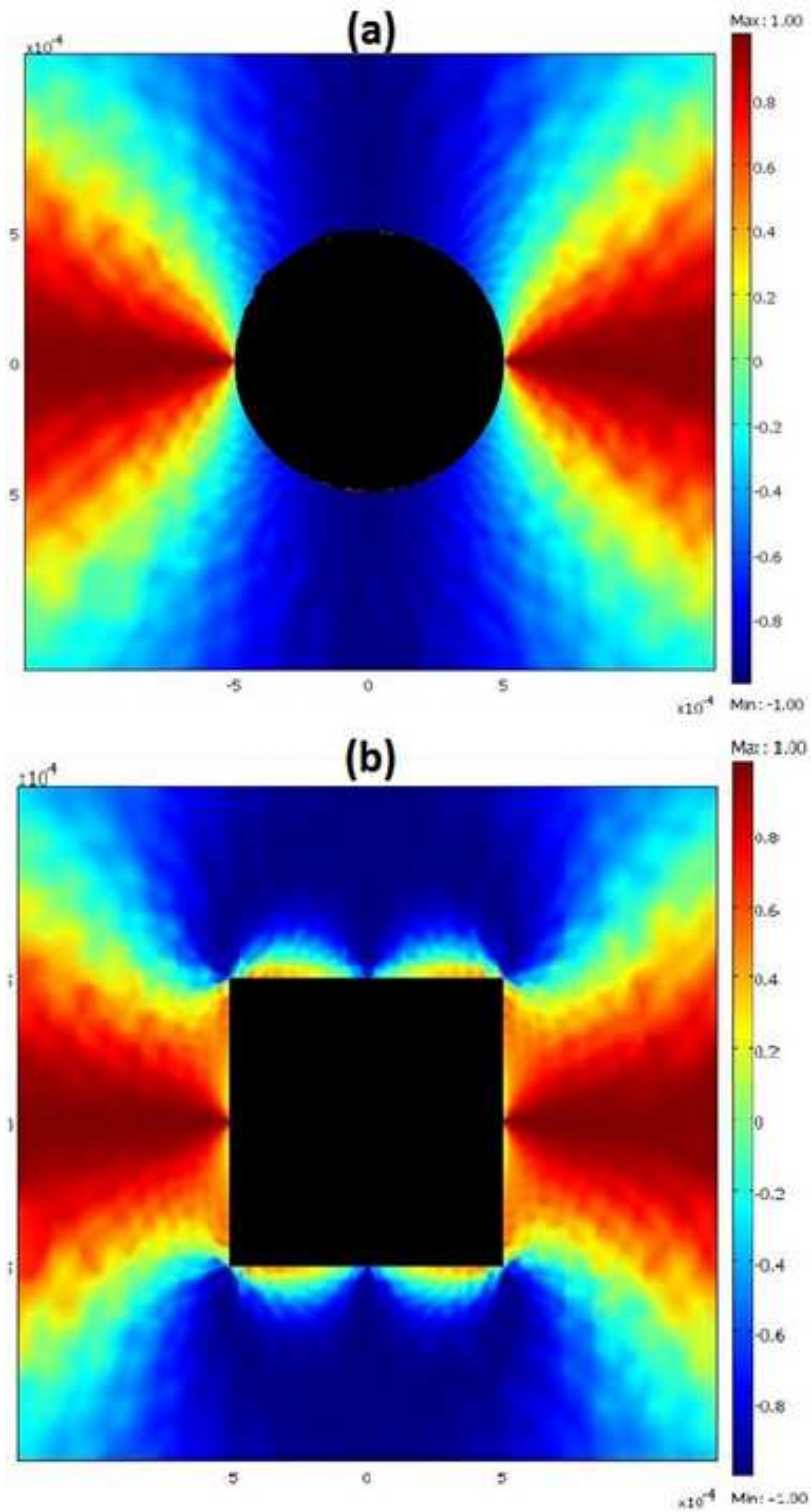
(a)
x10⁻⁴
Max: 1.00
0.8
0.6
0.4
0.2
0
-0.2
-0.4
-0.6
-0.8
Min: -1.00
5
0
5
-5
0
5
x10⁻⁴
(b)
x10⁻⁴
Max: 1.00
0.8
0.6
0.4
0.2
0
-0.2
-0.4
-0.6
-0.8
Min: -1.00
5
0
5
x10⁻⁴

Figure 4

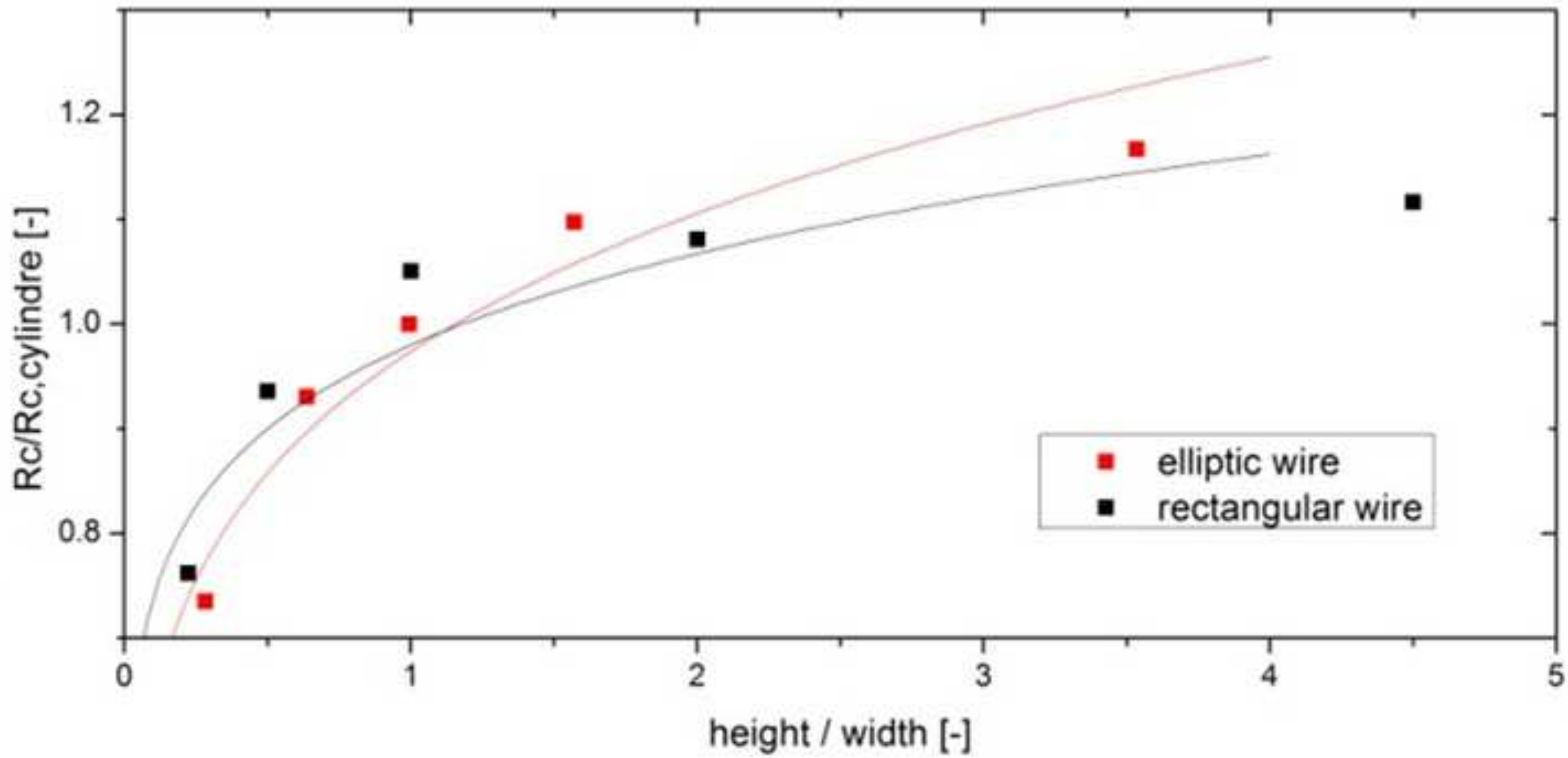

Rc/Rc,cylindre [-]
1.2
1.0
0.8
0
1
2
3
4
5
height / width [-]
elliptic wire
rectangular wire


(a)
(b)

Figure 6

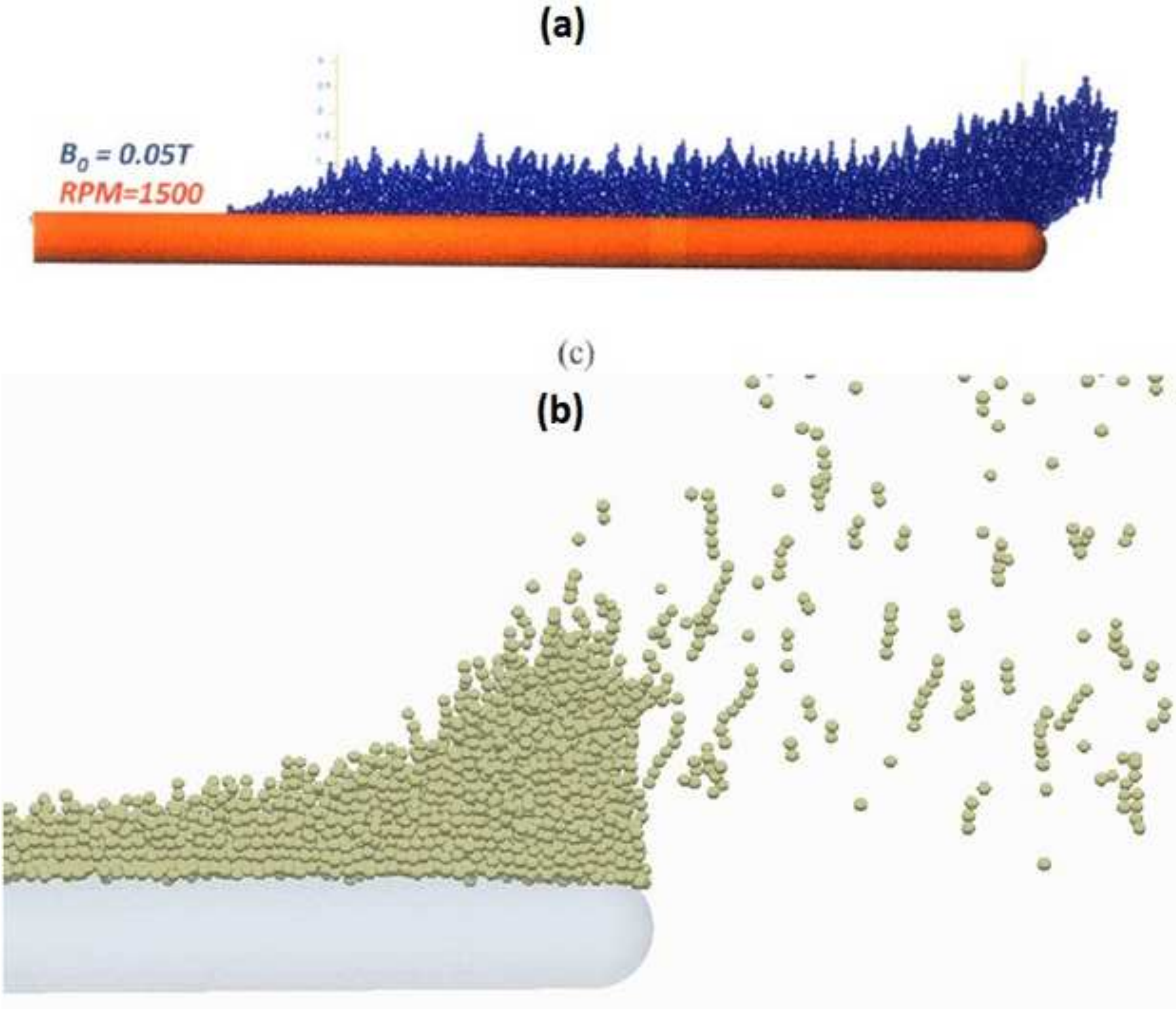

Figure 7

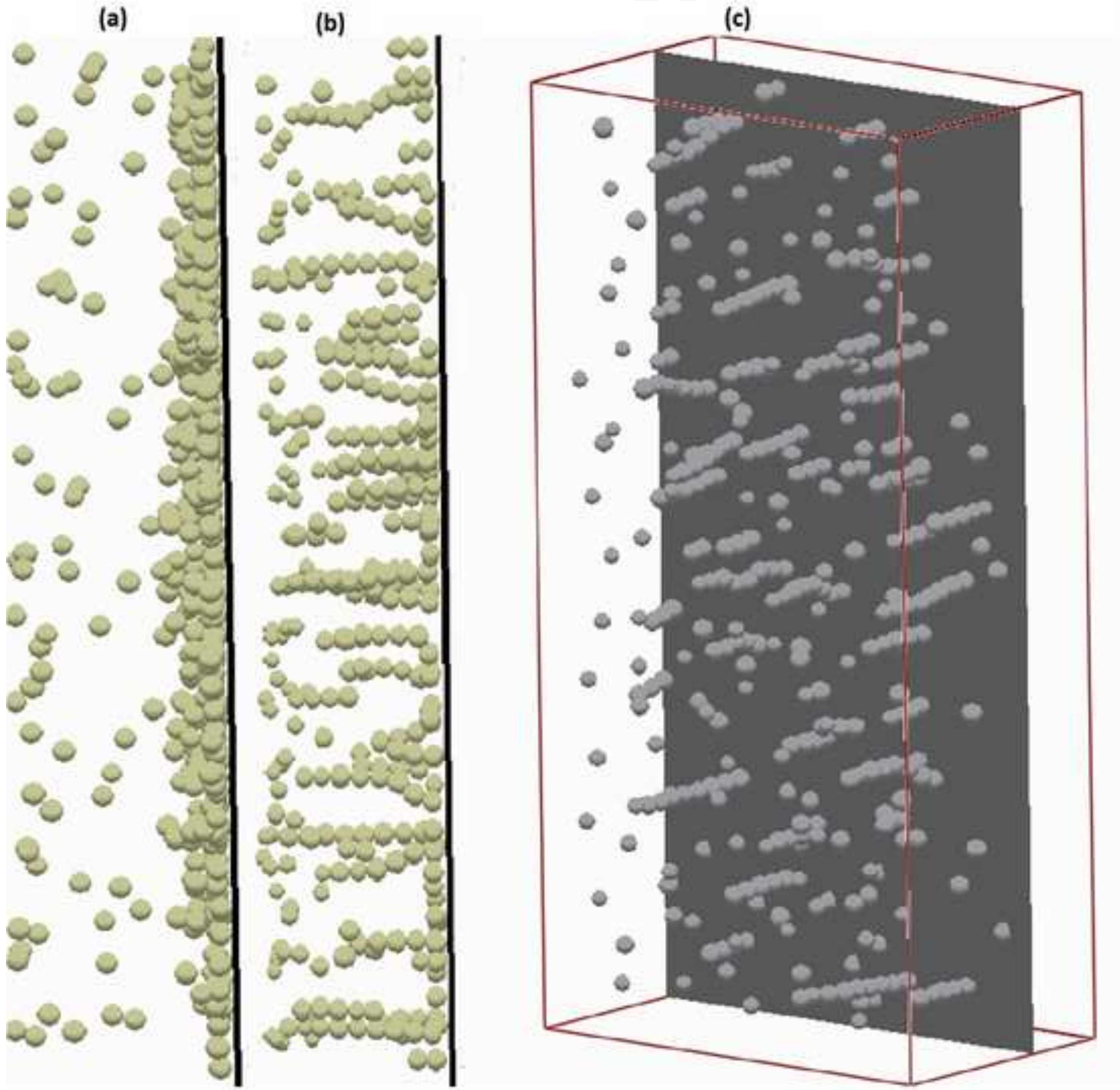

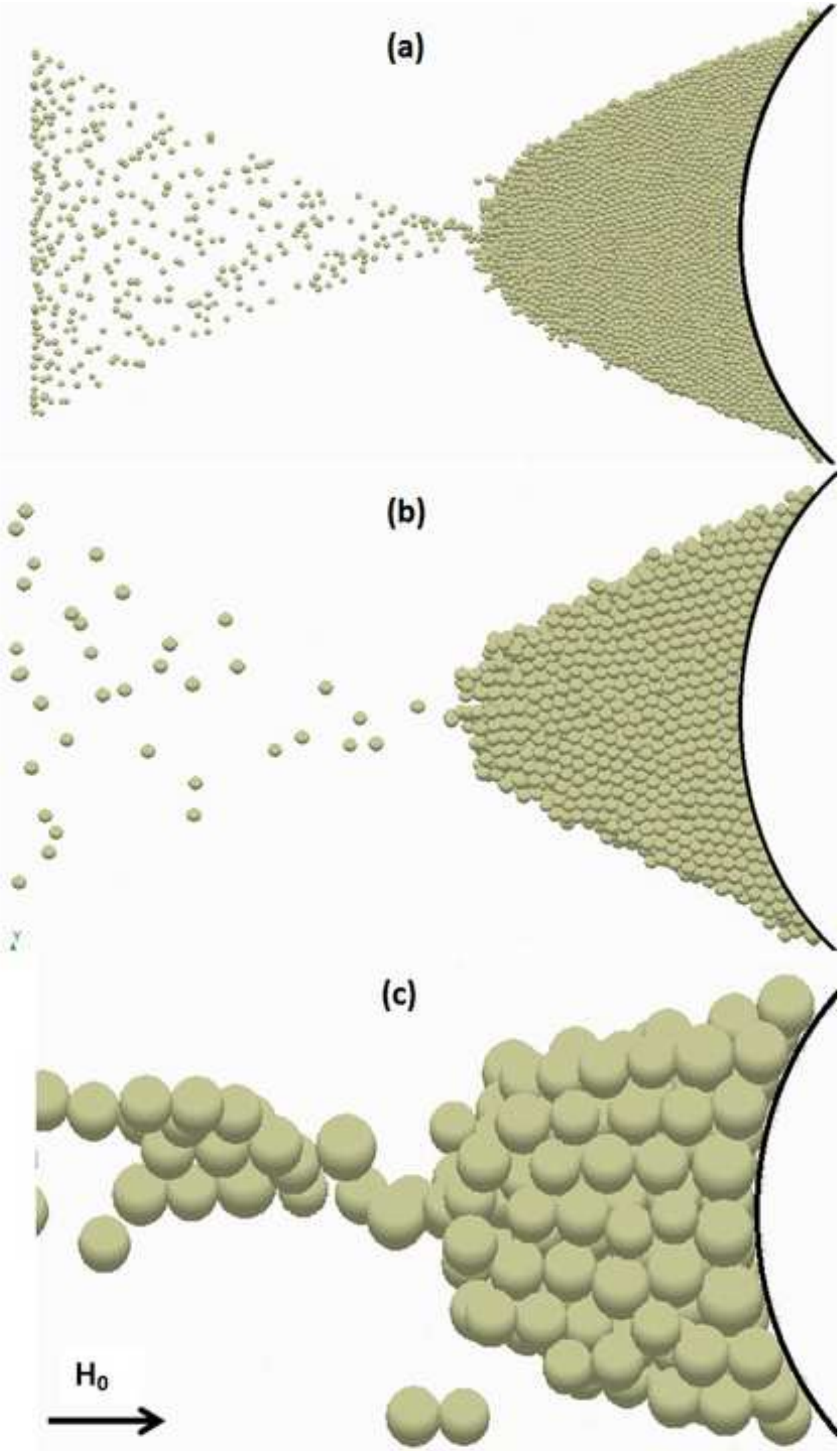
(a)
(b)
(c)
H₀

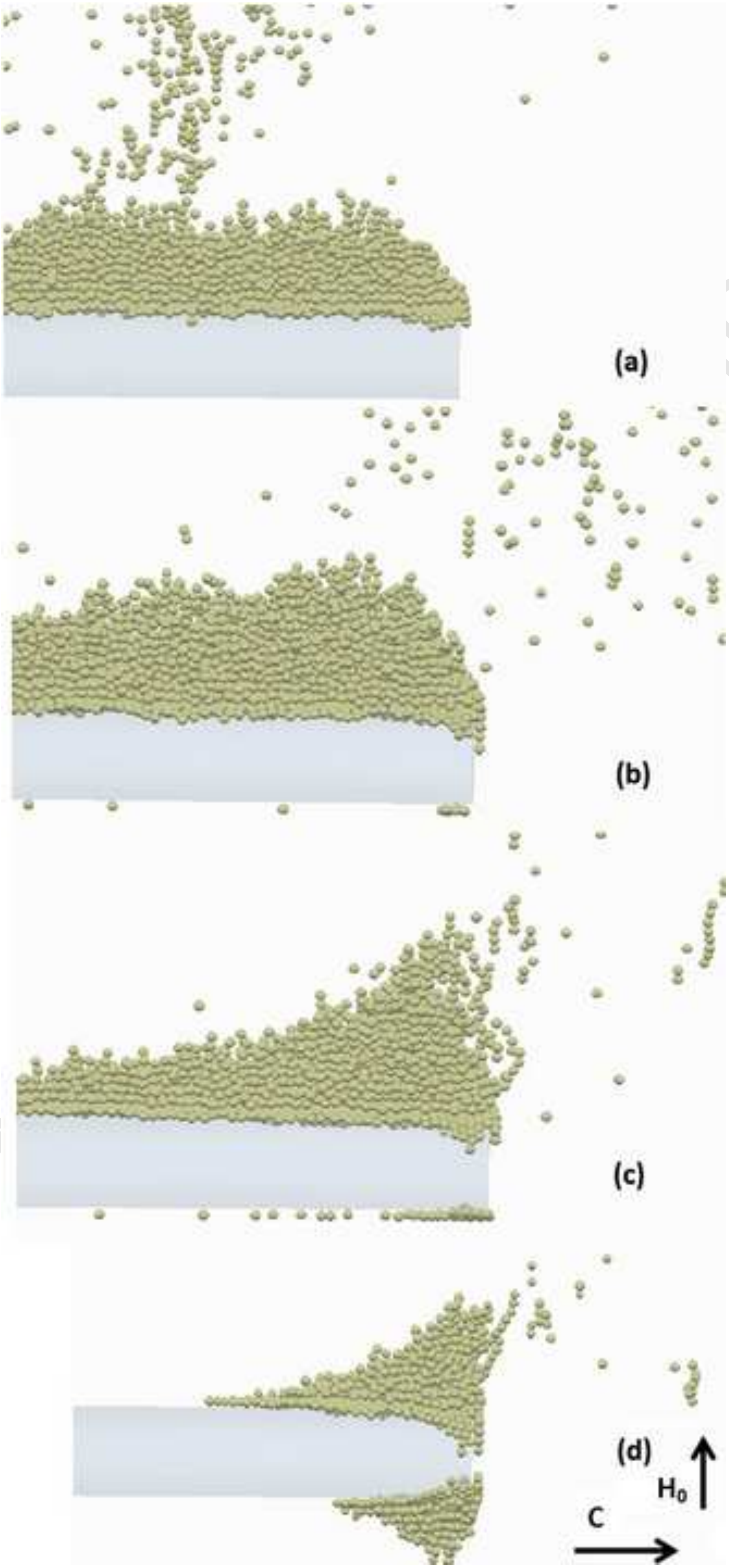
(a)
(b)
(c)
(d)
H0
C

Figure10

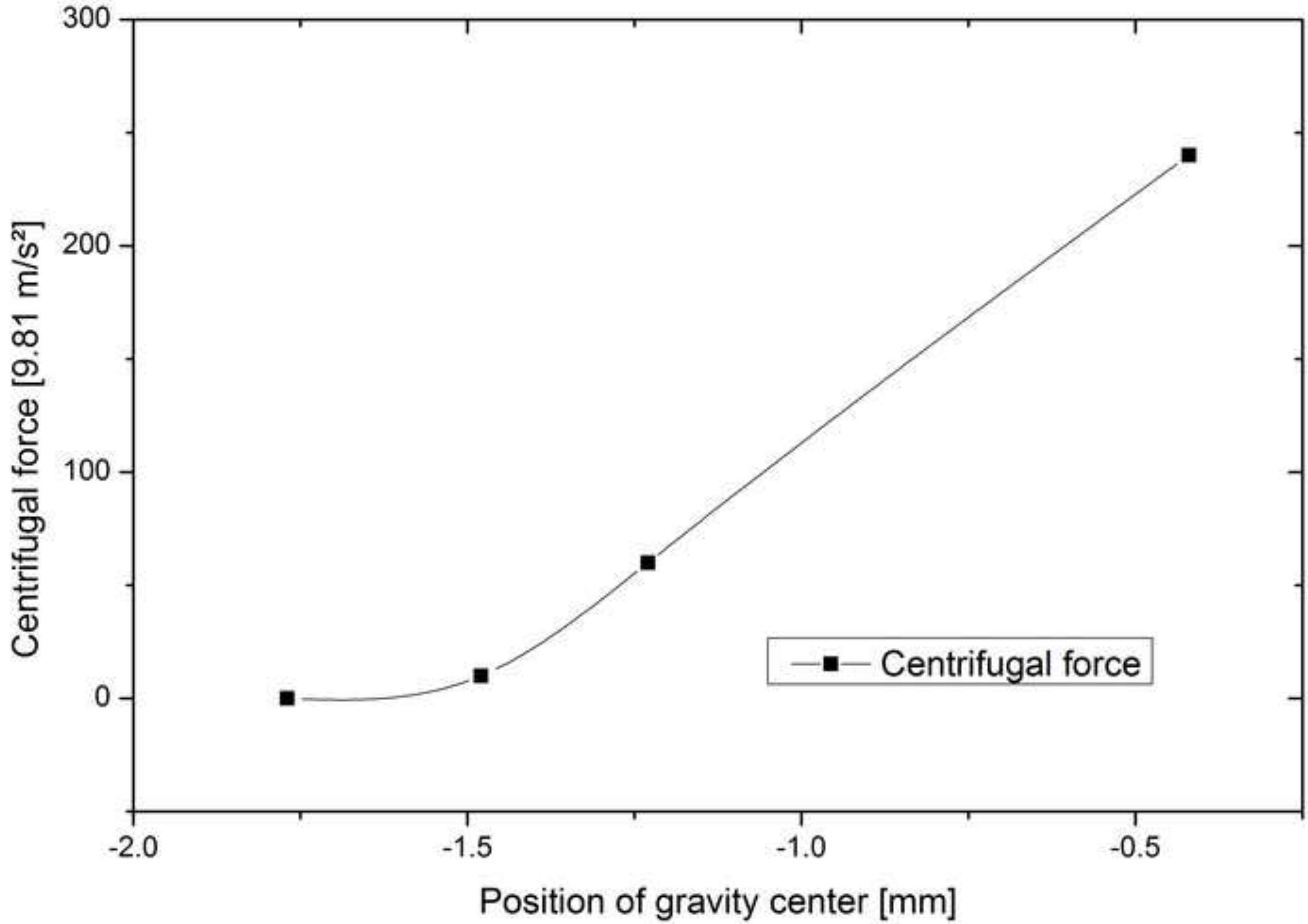

300
200
100
0
Centrifugal force [9.81 m/s²]
-2.0
-1.5
-1.0
-0.5
Position of gravity center [mm]
Centrifugal force

Figure11

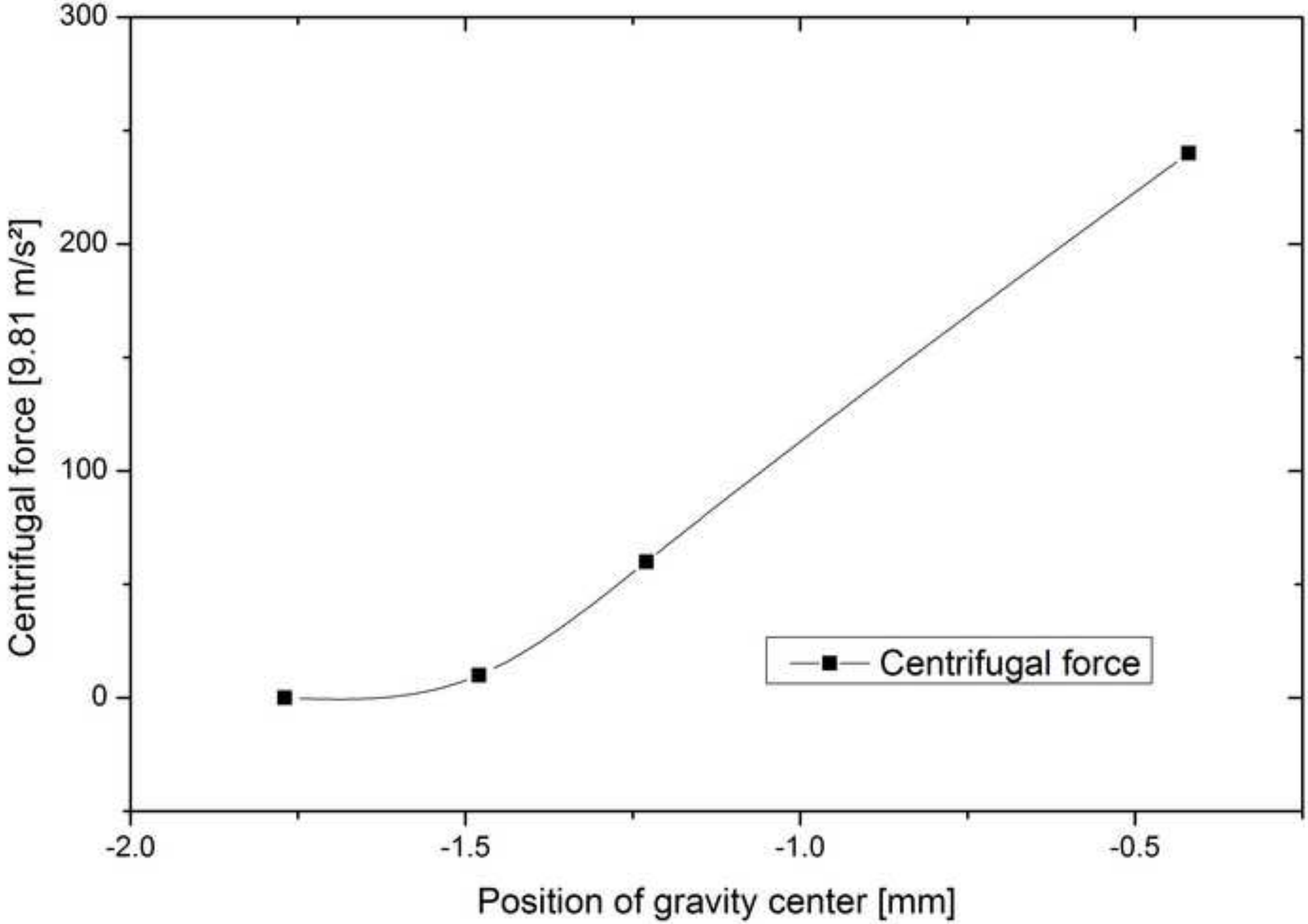

300
200
100
0
-2.0
-1.5
-1.0
-0.5
Centrifugal force [9.81 m/s²]
Position of gravity center [mm]
Centrifugal force